A Novel Approach to a Bifunctional Photosensitizer for Tumor Imaging and Phototherapy

Yihui Chen,[†] Amy Gryshuk,[†,‡] Samuel Achilefu,[§] Tymish Ohulchansky,[∥] William Potter,[†] Tuoxiu Zhong,[⊥] Janet Morgan,[†] Britton Chance,[⊥] Paras N. Prasad,[∥] Barbara W. Henderson,[†] Allan Oseroff,[‡] and Ravindra K. Pandey*[,†,§]

PDT Center, Cell Stress Biology, Roswell Park Cancer Institute, Buffalo, New York 14263, Department of Dermatology, Roswell Park Cancer Institute, Buffalo, New York 14263, Department of Radiology, Washington University School of Medicine, St. Louis, Missouri 63110, Department of Chemistry, State University of New York, Buffalo, New York 14221, and Department of Biophysics, Anatomy Chemistry Building, University of Pennsylvania, Philadelphia, Pennsylvania. Received June 20, 2005; Revised Manuscript Received July 20, 2005

Optical imaging has attracted a great attention for studying molecular recognitions because minute fluorescent tracers can be detected in homogeneous and heterogeneous media with existing laboratory instruments. In our preliminary study, a clinically relevant photosensitizer (HPPH, a chlorophyll-a analog) was linked with a cyanine dye (with required photophysical characteristics but limited tumor selectivity), and the resulting conjugate was found to be an efficient tumor imaging (fluorescence imaging) and photosensitizing agent. Compared to HPPH, the presence of the cyanine dye moiety in the conjugate produced a significantly higher uptake in tumor than skin. At a therapeutic/imaging dose, the conjugate did not show any significant skin phototoxicity, a major drawback associated with most of the porphyrin-based photosensitizers. These results suggest that tumor-avid porphyrin-based compounds can be used as "vehicles" to deliver the desired fluorescent agent(s) to tumor. The development of tumor imaging or improved photodynamic therapy agent(s) by itself represents an important step, but a dual function agent (fluorescence imaging and photodynamic therapy) provides the potential for tumor detection and targeted photodynamic therapy, combining two modalities into a single cost-effective "see and treat" approach.

INTRODUCTION

As photosensitizing agents, porphyrin-based compounds have played a central role in photodynamic therapy (PDT), the sensitization of tumor tissue to destruction by light (*1*−*3*). Photofrin, which was developed in the Roswell Park Cancer Institute (RPCI), is being used worldwide for the treatment of a wide variety of solid tumors. In the US, Photofrin PDT is approved for the treatment of obstructive esophageal cancer, early- and late-state lung cancer, and high-grade dysplasia associated with Barretts esophagus (*4*). The demonstrated clinical usefulness of PDT has spawned the development of a large number of new photosensitizers, and numerous tetrapyrrole-based compounds have been synthesized in various laboratories (*5*, *6*). Since the introduction of first PDT drug Photofrin, there have been continuous efforts in various laboratories to improve photosensitizer's tumor selectivity and specificity (*7*). Tumor cells in general have nonspecific affinity for porphyrins, the mechanism of porphyrin retention in tumors is not well understood, although the balance between hydrophilicity and hydrophobicity is recognized as an important factor. Some attempts have been made to direct photosensitizers to a known cellular target by creating a photosensitizer conjugates, where the other molecule is a ligand specific to the target (*8*, *9*). Some other examples of such photosensitizers are: conjugates with cell-membrane cholesterol (*10*) antibody (*11*−*13*), chemotherapeutic agents (*14*), etc. Certain proteins and microspheres were also made to improve the pharmacology of the compounds (*15*, *16*). These strategies seldom work well because the pharmacological properties of both compounds are drastically altered.

At RPCI, we have identified highly promising photosensitizing agents among a series of alkyl ether analogues of pyropheophorbide-a, (665 nm) (*17*, *18*), purpurinimides (705 nm) (*19*−*22*), and bacteriopurpurinimides (796 nm) (*23*−*25*) on the basis of quantitative structure−activity relationship (SAR) and/or SAR studies. One of the compounds in a pyropheophorbide-a series [3-devinyl-3-(1-hexyloxy)ethyl analogue (HPPH)] is currently in Phase I/II clinical trials at RPCI for the treatment of esophageal, lung, and cutaneous tumors (*26*−*27*).

Porphyrins and related compounds have also been investigated for use in optical diagnostic technologies based on their fluorescent properties, e.g., fluorescence being exploited as a possible technique for guidance of surgical intervention (*28*). In such surgical-assist applications, the ability to provide real-time information about surgical margins would be highly useful. Unfortunately, despite the attractiveness of the porphyrin-based compounds as photosensitizers for PDT, most of these compounds do not possess the excitation and emission spectra favorable for fluorescent contrast agents for imaging deep tissues. First, to maximize penetration depth into tissues, excitation between 750 and 800 nm

* To whom correspondence should be addressed. E-mail: ravindra.pandey@roswellpark.org. Phone: 716-845-3203. Fax: 716-845-8920.

[†] PDT Center, Cell Stress Biology, Roswell Park Cancer Institute.

[‡] Department of Dermatology, Roswell Park Cancer Institute.

[§] Washington University School of Medicine.

[∥] SUNY Buffalo.

[⊥] University of Pennsylvania.

10.1021/bc050177o CCC: $30.25
Published on Web 09/03/2005

is preferred and the Stokes shift must be large to enable discrimination of the small fluorescent component from the overwhelming large component of excitation light. An insufficient Stokes shift of 10−15 nm complicates the process of rejecting multiply scattered light, as the efficiency of the filters cannot be guaranteed. For these reasons, the usefulness of PDT agents for contrast is largely limited to superficial epithelial linings of accessible tissues.

In recent years, a number of optical imaging approaches have been reported (*29*). These techniques rely on fluorescence, reflectance, absorption, or bioluminescence as the source of contrast, while imaging systems can be based on diffuse optical tomography, surface-weighted imaging, phase-array detection, confocal imaging, multiphoton imaging, or microscopic imaging with intravital microscopy. However, with the exception of near-infrared (NIR) fluorescence imaging (*30*) and superficial confocal and two-photon imaging, these techniques currently are limited to experimental imaging to small animals. Unlike fluorescence microscopy of cells or thin-tissue samples, in vivo imaging is preferably performed in the NIR region (700−900 nm) because of more efficient tissue penetration of photons and minimal auto fluorescence in this region (*31*). Recently, this technology has been extended to in vivo imaging of biological targets and disease. It has been shown that frequency−domain photon migration (FDPM) with an image-intensified charge-coupled device (CCD) can be used for the detection of diseased tissues in vivo using fluorescent contrast agents (*32*). A number of different NIR fluorochromes such as cyanine dyes have been described with variable stabilities, quantum efficiencies, and ease of synthesis (*33*, *34*). Despite their excellent photophysical properties, except a few folic acid (*35*) or certain peptide-linked (*36*) cyanine dyes, most of them (e.g., indocyanine green) are not tumor specific and are eliminated rapidly from the organism. By realization of the importance of porphyrin-based compounds in tumor avidity and photosensitizing efficacy and the advantages of cyanine dyes for tumor imaging due to their inherent characteristic of NIR absorbance and emission, we were interested in designing "bifunctional agents" consisting of these two chromophores, which could produce the desired photophysical properties suitable for both tumor detection by optical imaging as well as therapy (PDT). Such image-guided PDT would represent a new paradigm for tumor treatment. To provide a proof of principle concept, we have prepared and preliminarily evaluated a conjugate comprised of the photosensitizer HPPH and cyanine dye IR820.

EXPERIMENTAL PROCEDURES

For ^{1}H NMR data, chemical shifts are expressed in ppm with reference to trimethylsilane (0.00 ppm). Column chromatographic separations were performed over silica gel 60 (70−230 mesh) or neutral alumina (Grade III (6% water), ∼150 mesh). Preparative thin-layer chromatography (TLC) was performed on silica 20 × 20 cm^2 TLC plates. The cyanine dye 1 was purchased from Aldrich Chemicals.

Cyanine Dye 3. Compound **1** (60 mg) and 4-aminothiophenol (60 mg) were dissolved in dry DMF and stirred overnight. DMF was removed by high vacuum, the residue was purified by chromatography using MeOH/CH_2Cl_2 (1:3) as the eluting solvent system, and **3** was obtained in ∼80% yield. NMR [MeOH (d4)], δ (ppm) 9.0 (d, 2H, H−a), 8.2 (d, 2H, H−b), 8.0 (t, 4H, H−c), 7.62 (d, 4H, H−d), 7.48 (2d overlapped to be triplet, 2H, H−e), 7.12 (d, 2H, H−f), 6.70 (d, 2H, H−g), 6.35 (d, 2H, H−h), 4.30 (t, 4H, H−i), 2.95 (t, 4H, H−j), 2.80 (m, 4H, H−k), 2.00 (m, 10H, 4H for H−l, 6H for m, n, o), 1.90 (s, 12H, H−p), 1.30 (s, H−q). MS for **3**: calcd $C_{52}H_{56}N_3NaO_6S_3$, 937; found, 937. High resolution (HR) MS for **3**: calcd $C_{52}H56N_3NaO_6S_3$, 937.3229; found, MH^+, $C_{52}H_{57}N_3NaO_6S_3$, 938.3320.

HPPH−Cyanine Dye Conjugate 5. HPPH **4** (100 mg) and DCC (110 mg) were dissolved in 1 mL of dry DMF and stirred for 10 min, and the solution of **3** (145 mg) in DMF (2 mL) and 10 mg DMAP were added. Twenty-four hours later, the reaction mixture was worked up. The residue was purified by chromatography using MeOH/CH_2Cl_2 (1:3) as the eluting solvent system, and **5** was obtained in ∼65% yield. UV−vis in H_2O: 848 nm (ϵ = 97547), 664 nm (ϵ = 53800), 413 nm (ϵ = 101456). UV−vis in MeOH: 833 nm (ϵ = 207455), 660 nm (ϵ = 53856), 408 nm (ϵ = 95222). NMR ($CHCl_3$) δ (ppm) for compound **5**: 9.47 (s, 1H, meso-H in HPPH part), 8.46 (s, 1H, meso-H in HPPH part), 8.35 (br-s, 3H, 1H for meso-H in HPPH part, 2H for H−a), 7.50 (m, 5H, 1H for H−b, 4H for H−c), 7.30 (m, 3H, 1H for H−b, 2H for H−e), 7.20 (s, 2H, H−f), 7.05 (s, 4H, H−d), 6.85 (s, 2H, H−g), 6.61 (s, 2H, H−h), 5.70 (br, 3H, 1H for H-3^1, 1H for H-17, 1H for H-18), 4.54 (br-doublet, 1H, H-13^2), 4.22 (br, 2H, H−i), 3.66 (br, 2H, H−i), 3.20 (br, 9H, 5H for HPPH part: 3H for 7-CH_3, 2H for 3^1-OC*H*$_2$(CH$_2$)$_4$CH$_3$, 4H for H−j), 3.03 (m, 4H, H−k), 2.90 (s, 1H, −CON*H*), 2.72 (br, 7H, 2H for 8-C*H*$_2$CH$_3$, 2H for 17-CH_2CH_2CO-, 3H for 2-CH_3), 2.55 (br, 5H, 2H for 17-CH_2CH_2CO-, 3H for 12-CH_3), 1.88 (br, 3H, 3-$CHCH_3$), 1.72−0.72 (many multiples, 36 protons, 22 H for dye part: 12H for H−p, 4H for H−l, 6H for H−m, n, o; 14 H for HPPH part, 3H for 18-CH_3, 3 H for 8-CH_2C*H*$_3$, 8H for 3^1-OCH$_2$(C*H*$_2$)$_4$CH$_3$), 0.62 (m, 3H, 3^1-OCH$_2$(CH$_2$)$_4$C*H*$_3$. MS for **5**: calcd $C_{91}H_{102}N_7NaO_9S_3$, 1555.6; found, 1555.7. HRMS for **5**: calcd $C_{91}H_{102}N_7NaO_9S_3$, 1555.6798; found MH^+ $C_{91}H_{103}N_7NaO_9S_3$, 1555.6920.

Formulation of the Conjugates. HPPH and the corresponding cyanine dye conjugate were insoluble in water. Therefore, these compounds were formulated in 1% Tween-80/5% dextrose solution. The concentration of the final formulation was determined by following the Beer−Lambert's law. The stability and purity of the conjugates in formulation was ascertained by high-performance liquid chromatography analysis.

Photophysical Characterization. Photophysical properties of the synthesized conjugates were examined in different solvents (water, methanol, chloroform, etc., depending on solubility). Methods of electronic absorption and steady-state and time-resolved luminescence spectroscopy were used (*37*). Steady-state measurements were performed using a Shimadzu UV-3101PC spectrophotometer (absorption spectra) and Fluorolog-3 spectrofluorometer (Jobin Yvon) (fluorescence spectra). A SPEX 270M spectrometer (Jobin Yvon) equipped with an InGaAs photodetector (Electrooptical Systems Inc., USA) was used for acquisition of singlet oxygen emission spectra and dye emission in the NIR spectral range. A diode-pumped solid-state laser (Verdi, Coherent) at 532 nm was the excitation source in this case.

For the measurement of fluorescence decays, a Becker & Hickl Photon counting module (SPC-830), equipped with a fast PMT (Hamamatsu H7422) having a system response of about a 300-ps full width at half maximum, was used. A Ti:Sapphire laser (Tsunami from Spectra Physics) tunable in the range of 740−880 nm (∼100-fs pulses at 82 MHz) using BBO crystal and the obtained

light were used to excite the sample solution in a cuvette. A PHD-400-X high-speed photodiode module was used to provide a synchronization signal from the Ti:Sapphire laser.

Cell Line. For HPPH and the corresponding cyanine dye conjugate, RIF (radiation induced fibrosarcoma) cells were cultured in αMEM medium. Semiconfluent culture was used for in vitro studies of photosensitivity (survival studies) and drug localization as well as propagation of tumors in vivo by following the methodology routinely used in our laboratory.

Intracellular Localization of Conjugates. To determine subcellular localization, HPPH and the conjugate were co-incubated with organelle-specific fluorescent probes. RIF cells were seeded at 2×10^5 on poly-L-lysine-coated cover slips in six-well plates and cultured for 24 h to allow attachment and spreading. HPPH or conjugates at appropriate concentrations (typically 0.5−2 μM) were added to cells in culture medium, and the cells incubated for 3 or 24 h at 37 °C, 5% CO_2 in the dark. To determine subcellular localization, cells were co-incubated with fluorescent probes (Molecular Probes, Invitrogen Carlsbad, CA) known to target mitochondria (Rhodamine 123, 1 μM or Mitotracker Green, 200 nM) or lysosomes (yellow-green Fluospheres 0.1 μm diameter, 1:10 000 dilution). Mitotracker Green and Fluospheres were added 24 h prior to microscopy, the latter with gently rocking and the R-123 was added during the final 30 min of incubation. The cells were then rinsed briefly with phosphate-buffered saline (PBS) and examined immediately by fluorescence microscopy (Zeiss Axiovert 35, Carl Zeiss, Inc., Germany) with a 200-W mercury arc lamp light source.

Fluorescence was imaged with a CCD camera and intensifier as previously described (*38*) and processed with Metamorphose 4.5 (Universal Imaging Corp., Downington, PA). Images of photosensitizers and co-localizing dyes in the same field were taken in rapid succession. Photosensitizers were detected using a combination of 530−580-nm excitation and 600-nm dichroic/615-nm long-pass emission filters. R-123, Mitotracker Green, and Fluospheres were detected using 445−490-nm excitation and 510-dichroic/520−560-nm long pass/emission filters.

In vitro Photosensitizing Efficacy. RIF tumor cells (*18*) were cultured in αMEM (Invitrogen, Carlsbad, CA) supplemented with 10% fetal calf serum (Herndon,VA) in 100% humidity with 5% CO_2. Cells were harvested and used for in vitro assays in the log phase of growth. In a typical experiment, cells will be seeded in replicates at 5×10^4 cells/well in 96-well plates. Cells were incubated overnight before adding the desired conjugate at variable concentrations (0.125, to 4.0 μM). After 3 or 24 h incubation with the drug in the dark, cells were exposed to laser light at the longest wavelength absorption peak of the conjugate to deliver doses of 0.5−4 J/cm^2. After light treatment, fresh medium was added and the cells were incubated for 48 h. Phototoxicity for each photosensitizer was assessed after 48 h by comparing growth of treated cells to control cells (no drug, no light) as measured by formazan production using the 3-[4,5-dimethylthiazol-2-yl]-2,5-diphenylyetrazolium bromide (MTT) assay (*39*). Ten microliters of MTT (Sigma, St. Louis, MO) at 4 mg mL^{-1} in PBS was added, and the cells were incubated for 4 h. The medium was removed and the formazan crystals were dissolved in dimethyl sulfoxide (DMSO, FisherBiotech, Fair Lawn, NJ) at 100 μL per well. Formazan absorbance was read on a 96-well plate reader (Titertek Multiskan Plus MK II Miles Inc.) at 560 nm.

Tumor Uptake by in vivo Reflectance Spectroscopy. Tumor-bearing mice were anesthetized using ketamine/xylazine (2.2 mg/20 g mouse). The optical density as a function of wavelength was recorded before the intravenous (iv) injection of the conjugate (*40*). The monochromator was set to the expected longest wavelength of the experimental drug's in vitro absorption spectrum. The drugs were then administered by tail vein injection, and the light signal was recorded. The second spectrum was altered by the presence of drug in the tumor. This in vivo drug absorption spectrum was best displayed by taking the ratio of the post-injection spectrum to the pre-injection spectrum. This ratio offered the same advantages as a double beam absorption spectrophotometer. Data obtained before drug administration represented the reference spectrum. The ratio of these two spectra was not influenced by the wavelength dependence of the instrument. As a safeguard against day-to-day or hour-to-hour drift in the total light output of the lamp, both spectra (before and after administration) were normalized by dividing the signal strength at a wavelength where the drug absorption is negligible. To determine the uptake/clearance of tumor vs skin, another probe was used to record the in vivo absorption spectrum of the compound present in skin.

In vivo Antitumor Effect. Photosensitizers were injected intravenously (tail vein) in approximately 0.2-mL volumes. Mice bearing transplantable tumors were restrained without anesthesia in Plexiglas holders designed to expose only the tumor and a 2−4-mm angular margin of skin to light. For mice bearing spontaneous tumors at unpredictable sites, light exposure was flexibly adjusted to accommodate exposure of these sites. The tumors were exposed with a laser light source at appropriate absorption wavelength (Spectra Physics coherent argon-pumping tunable dye lasers, ranging from 630 to 800 nm, and ILX Light wave laser diode controller containing diodes of desired wavelength). The drug and light dosimetry followed the experimental design outlined previously (*18*). A typical experiment was as follows: Day 0: implant tumor. Staging day: select mice with tumor measuring 4.5−5.5 mm (longest axis), prepare photosensitizers, record body weight, and inject test photosensitizer (iv). Treatment day (chosen based on prior tumor uptake data determined by in vivo reflectance spectroscopy): expose tumors to light, measure tumor dimensions (orthogonal diameters) by caliper every other day for tumor growth/regrowth assays. The tumor volume, V, is calculated with the formula $V = (lw^2/2)$, where l is the longest axis of the tumor and w is the axis perpendicular to l. Observe treatment field, i.e., record observations of edema, erythema, and escar formation. Record time to regrowth of tumors to 400 mm^3 (those mice in which there was no tumor regrowth for 90 days, accounted as cured mice). Mice were sacrificed for ethical consideration when tumors reach that volume (400 mm^3).

Normal Tissue Responses. Foot response was judged using a 0−3 scale. 0 = no apparent difference from normal, 0.1 = very slight edema, 0.3 = slight edema, 0.5 = moderate edema, 0.75 = large edema and/or slight erythema, 1.0 = large edema and/or erythema with exudate, 1.2 = moderate erythema, with slight scaly or crusty appearance, 1.5 = definite erythema with definite scaly or crusty appearance, 1.65 = slight damage and or slight fusion of toes, *2.0 = most toes fused but general shape unchanged, 2.5 = foot shapeless with no toes, 3.0 = only stub of foot remaining (*41*).

Assessment of Vascular Perfusion. Fluorescein was used as a marker for vascular perfusion or changes

thereof (*42*). At various time points after PDT exposures of normal skin, each mouse was given intravenous injection of 0.2 mg of fluorescein dye (10 mg of sodium fluorescein per milliliter of HBSS; Baker Chemical, Phillipsberg, NJ). Immediately thereafter, the animal's back was illuminated with UV light (Black-Ray longwave lamp, Ultra-Violet products, Inc., San Gabriel, CA), and the fluorescein distribution between the treatment area and surrounding skin was visualized and recorded. To quantify the vascular photosensitivity, the PDT light doses were adjusted by increments of 5−25 J cm^{-2} (λ_{ex}, 490 nm; λ_{em}, 520 nm) from a base dose where no dye exclusion was observed until a minimum light dose to give complete exclusion of fluorescein from the treatment area, i.e., occlusion of the skin vasculature was established (*43*).

High-Resolution Tumor Imaging. Frozen tumor tissue was embedded in an ethanol−glycerol−water mixture (freezing point: −30 °C) and mounted in a redox machine: a 3D, high-resolution cryofluorometer scan system for 3D surface fluorometric scanning (*28*). The frozen tumor sample was ground flat for imaging before it was further ground down to obtain images usually every 100 μm. A bifurcated optical fiber bundle (7 quartz fibers, 70 μm core diameter for each, 1 fiber for emission in center, 6 fibers for excitation around the emission fiber) stepped across the tissue surface at a fixed distance from the tissue surface (70 μm). The filters for each substance's fluorescence excitation and emission were chosen based on the absorption and emission spectra of each fluorophores. By use of a mercury arc lamp as the excitation light source, the fluorescent signals of conjugate **5** (filters: ex, 405DF40; em, 670DF20), cyanine dye (filters: ex, 780; em, 856) were imaged for each depth of the tumor. The scanning was performed at 128 × 128 steps that covered 1.024 × 1.024 cm^2 area (80 μm per step). The fluorescence signals were recorded digitally on a PC and reconstructed later with MATLAB.

Whole-Body Imaging and Biodistribution Assays. Animal studies were performed in accordance with the Guide for the Use of Laboratory Animals. A noninvasive in vivo continuous wave fluorescence imaging apparatus was used to assess the localization and distribution of the conjugates, as described previously (*44*, *45*). Briefly, light from two laser diodes of nominal wavelength 780 or 808 nm and nominal power of 50 mW was launched into fiber optic bundles. The nominal 50 mW of incident power was reduced to about 20 mW at the output of the fiber optic bundle. A defocusing lens in position after the bundle was used to expand the beam such that nearly the whole mouse was illuminated. Digital images were recorded with a Photometrics CoolSNAP HQ CCD camera (12 bit, 1024 × 1024 pixels, back illuminated, thermoelectric Peltier cooled with forced air) equipped with an 830−870-nm interference filter. Images were acquired and processed using WinView software from Princeton Instruments. Data analysis consists of subtracting (pixel by pixel) the pre-injection or background image from the post-injection images and displaying the false color results. Integration of the relative fluorescence intensities of tumor vs surrounding tissues indicated qualitatively the extent of selective uptake of the molecular probe. Typically, the probes were administered via the lateral tail vein at dosages of 0.3 and 3.5 μmol/kg body weight of the mouse (depending on optimal therapeutic dose). Images were taken at 24, 48, and 72 h post-injection of the probe. The tumor-bearing mice (3 mice/group) were anesthetized with ketamine/xylazine via intraperitonial injection, and the conjugate was administered intravenously at a therapeutic dose. At the best imaging time (24 or 48 h), the animal was euthanized and selected organs were removed, washed, and placed on a dark background for fluorescence imaging. Tissue parts, instead of whole organs, were used to determine the relative fluorescence intensity in each organ to minimize problems associated with depth-dependent nonlinear fluorescence emission. A statistical program in the WinView package was used to estimate the mean fluorescence intensity per organ part.

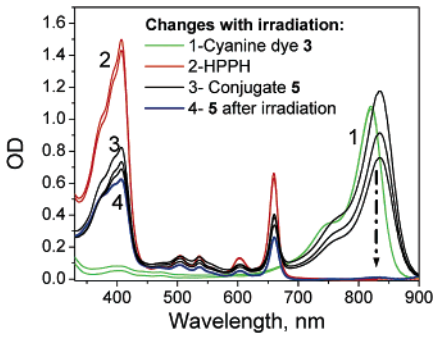

Figure 1. The absorption spectra of compounds **3**−**5** in dichloromethane. In conjugate **5**, irradiation of the HPPH absorption at 660 nm caused a significant decrease in the absorption of the cyanine dye at 831 nm (broad peak) and finally its complete photodestruction with a simultaneous increase in the intensity of HPPH absorption.

RESULTS AND DISCUSSION

Chemistry. As proof-of-principle of our approach to develop compounds with both imaging and therapeutic capabilities, we synthesized a conjugate **5** consisting of a highly effective photosensitizer, HPPH, and a cyanine dye exhibiting long wavelength absorption at 660 and 836 nm, respectively, with a strong emission at 865 m. In our preliminary study, the conjugate, designated as our lead compound, was evaluated for its photophysical characteristics, intracellular localization, in vivo tumor vs skin uptake, in vitro/in vivo photosensitizing efficacy, whole body imaging, biodistribution characteristics, and in vivo mechanistic and skin phototoxicity. These studies support the validity of our approach. The results are summarized as follows.

Synthesis of HPPH−Cyanine Dye Conjugate. The cyanine dye, namely, 2-[2-[2-chloro-3-[{1,3-dihydro-1,1-dimethyl-3-(4-sulfobutyl)-2H-benzo-(e)-indol-2-ylidene]-ethyl-indene]-1-cyclohexen-1-yl}ethenyl]-1,1-dimethyl-3-(4-sulfobutyl)-1H-benzo[e] indolium hydroxide, inner salt, sodium salt] **1** was first reacted with 4-aminophenylthiol and the corresponding 2-(4-aminophenylthioether) analogue **3** was isolated in 80% yield. Reaction of **3** with HPPH **4** (HPPH was prepared from chlorophyll-a by following the methodology developed in our laboratory) in the presence of DCC, and the desired HPPH−cyanine dye conjugate **5** was isolated in good yield (65%) (Scheme 1). UV, NMR, and mass spectrometry analyses confirmed the structure of the desired conjugate. The photophysical characteristic of the conjugate was first investigated before comparing its in vitro and in vivo photosensitizing efficacies and tumor-imaging capability with cyanine dye **3** and HPPH **4**.

Photophysical Studies. The electronic absorption spectrum of the conjugate **5** contains the characteristic absorption bands for two chromophores, i.e., HPPH **4** and the modified cyanine dye **3** (see Figure 1). The absorption characteristics of the HPPH moiety in the conjugate **5** remains practically unchanged in respect to the free HPPH.

Scheme 1. Synthesis of Conjugate 5

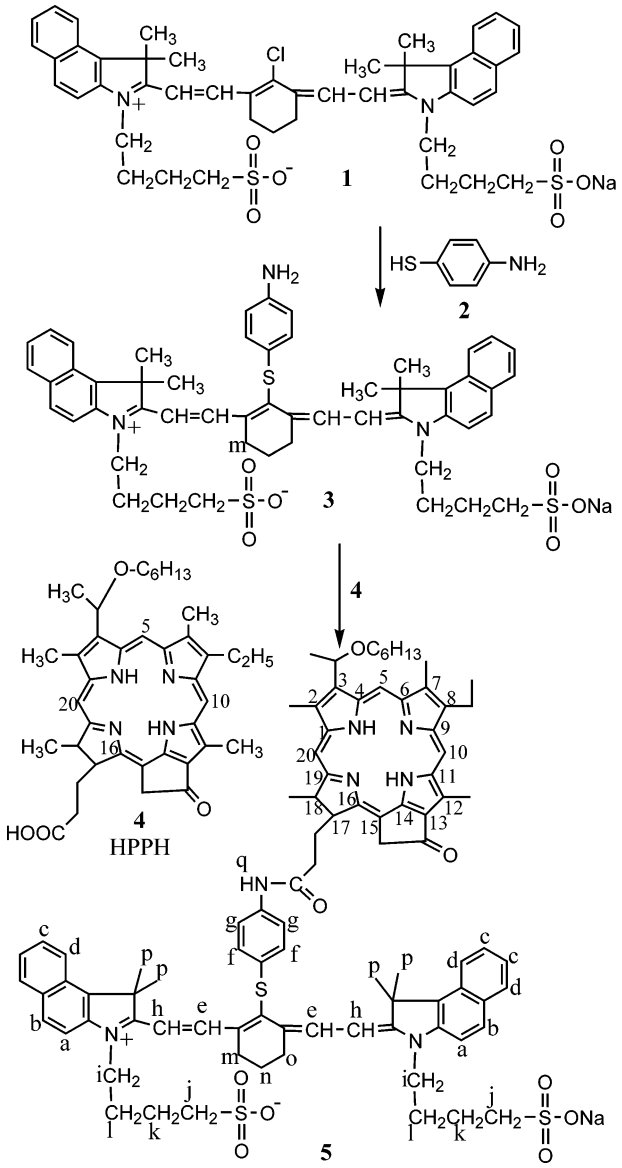

Compared to the free cyanine dye, in conjugate **5**, the absorption band for the cyanine dye moiety was found to be red shifted by 15 nm (820−835 in methanol), which is apparently associated with a change in environmental polarity caused by the presence of the HPPH moiety. Because of the similarity of the absorption spectra of HPPH and cyanine dye in conjugate **5** with respect to individual chromophores (without formation of any new absorption bands), it appears that the HPPH and cyanine dye π-electron systems in conjugate **5** absorb light practically independently. At the same absorption at the wavelength of excitation, the fluorescence intensity from the HPPH moiety in **5** was found to be significantly lower than observed for free HPPH. The electronic excitation energy transfer most probably occurs in **5** from the HPPH (donor) to the cyanine dye (acceptor). In methanol solution, irradiation of conjugate **5** at 532 nm (i.e., activation of HPPH) caused photolysis of cyanine dye moiety, and significant changes were observed in both absorption and fluorescence spectra. With increasing time of irradiation, absorption and fluorescence from the cyanine dye moiety at 835 and 875 nm, respectively, decreased, with a simultaneous increase in the intensity of fluorescence/absorption of the HPPH moiety. This is certainly due to the destruction of the π-electron system of the acceptor with subsequent discontinuation of a channel for the electronic excitation energy transfer. Comparison of the absorbance intensity ratios between nonirradiated vs irradiated −HPPH conjugate **5** (Figure 1) shows that the absorbance intensity of HPPH was increased by approximately 3-fold as a result of irradiation at 665 nm.

It was observed that, during irradiation (at 660 nm), the destruction of the cyanine dye moiety in conjugate **5** takes place continuously with a simultaneous increase in $^1O_2$ production (not shown). What is interesting to note is that the noticeable destruction of the cyanine dye moiety was observed only by excitation of the HPPH moiety and that the compound was found to be quite stable on exciting at the wavelengths that correspond to the cyanine dye moiety. Therefore, conjugate **5** shows an interesting characteristic for a suitable "bifunctional agent" that could be used for tumor imaging and therapy. Further detailed in vitro and in vivo photophysical investigations including the electrochemical studies with conjugate **5** are currently in progress and will be published elsewhere.

In vitro Photosensitizing Efficacy. The in vitro efficacy of the conjugate was determined in RIF cells, and the conjugate **5** was evaluated by performing two sets of experiments. After incubating the cells in the dark at 37 °C with 5 at various drug concentrations for 24 h, the medium was replaced with drug-free complete medium and cells were exposed to light either at 665 or 810 nm and the in vitro photosensitizing efficacy was determined by MTT assay (*39*).

In the first set of experiments, the photosensitizing activity of conjugate **5** was compared with HPPH. The cells were exposed to 665-nm laser light. As can be seen from Figure 2A, compared to HPPH the conjugate **5** was found to be equally effective. Interestingly, in a second set of experiments, on exposing cells to 810-nm diode light there was not any significant cell kill for either the cyanine dye **3** or conjugate **5** (Figure 2B). These results further confirm that the cyanine dye part of the moiety in conjugate **5** does not produce any significant singlet oxygen, which is a key cytotoxic agent for the destruction of tumor cells by PDT.

Comparative Intracellular Localization. Mitochondria have been identified as the most sensitive intracellular targets for PDT (*43*, *44*), and HPPH has been found to localize to the mitochondria (*46*). We therefore determined whether the conjugation of HPPH to cyanine dye affected the subcellular distribution of the photosensitizer. The localization of HPPH **4** and the corresponding cyanine dye conjugate **5** was investigated by co-incubating photosensitized RIF cells with Mitotracker Green (Molecular Probes, Eugene, OR) or Fluospheres (0.1 μm diameter latex heads labeled withfluorescein isothiocyanate 1/10 000 dilution by Molecular Probes, Eugene, OR), which target mitochondria and lysosomes, respectively. Fluorescence was imaged with a CCD camera and intensifier, and the images of photosensitizers and Mitotracker Green or Fluosphere localization were taken in rapid succession by following the literature procedure (*44*, *45*). From the results summarized in Figure 3, the imaging data clearly indicate that the HPPH and the conjugate localize in the same subcellular region as the mitochondrial marker, suggesting their affinity to mitochondria. The results obtained by using Fluospheres as a counterstain did not show any lysosomal colocalization (data not shown).

In vivo Photosensitizing Activity. The in vivo photosensitizing efficacy was determined in C3H mice transplanted with RIF tumors. Once the tumors reached

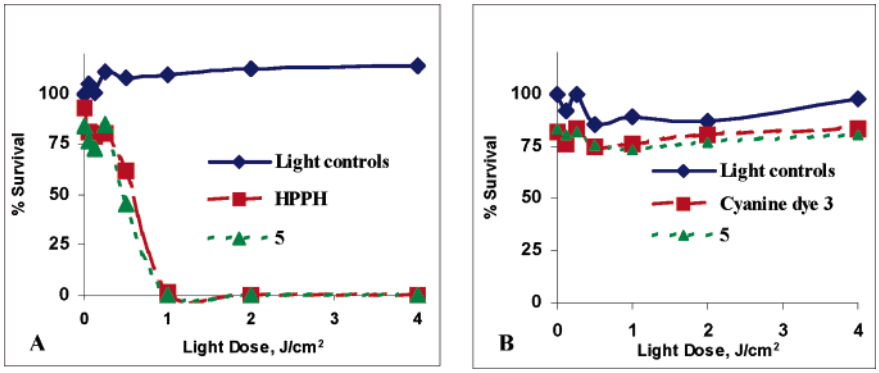

Figure 2. Comparative in vitro photosensitizing efficacy of the cyanine dye **3**, HPPH, and the corresponding cyanine dye conjugate **5** at equimolar concentration (0.6 μM) in RIF tumor cells: (A) the cells incunated with HPPH and the conjugate **5** were exposed to light at 665 nm and (B) the cyanine dye **3** and the conjugate **5** were exposed to light at 810 nm at variable light doses.

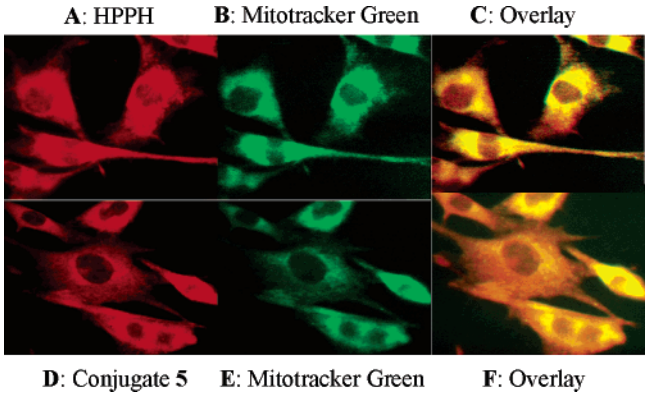

Figure 3. Comparative localization (false images) of HPPH **4** and conjugate **5** with Mitotracker Green (mitochondrial probe) in RIF cells after incubating for 24 h (for details, see the text).

4−5 mm^3, they were exposed to light (135 J/cm^2) at 24 h after injection of the conjugate at variable drug doses. The tumor growth (to reach >400 mm^3) was monitored daily for 30−90 days. As can be seen from Figure 4, clear dose−response relationships were observed, with a dose of 3.5 μmol/kg of the conjugate being highly effective in controlling the tumor regrowth (8/10 mice were tumor free at day 90). This therapeutic dose was subsequently chosen for tumor imaging.

High-Resolution Tumor Image. We have assessed the three-dimensional distribution of conjugate **5** in frozen sections of the RIF tumor, by means of fluorescence spectrophotometric imaging of successive slices through the frozen tissue block (*47*). Figure 5 illustrates a diffuse, heterogeneous distribution of **5** with maximal levels at the growing edge of the tumor, particularly indicated in the 300- and 900-μm sections, with little in the necrotic center. The histogram (D) for the distribution of conjugate **5** is broad Sand bimodal, ranging from 50 to >250 intensity values representing the low accumulation in the center compared to the viable periphery. The median tissue fluorescence in the absence of **5** was ~30 (C and F). The localized distribution of cyanine dye **3** is indicated in the same range. The dye is localized mainly in the tumor, both in the necrotic portion of the tumor and in the actively growing edge (see the 600-μm slice 3).

In vivo Imaging. Results of whole body fluorescence imaging (*48*) in the RIF tumor-bearing mouse, with excitation of the fluorescent cyanine dye moiety of conjugate **5** 24 h after administration, are shown in Figure 5. It was exciting to note that even at a dose of 0.3 μmol/kg, which was later found to be 8−10-fold less than the therapeutic dose, the conjugate showed significant tumor-imaging capability. Once the optimum therapeutic dose of 3.5 μmol/kg was determined, further imaging experiments were carried out to determine the time course of the tumor and the organ distribution of conjugate **5** in intact mice (Figure 5G) and in the isolated organs (Figure 6).

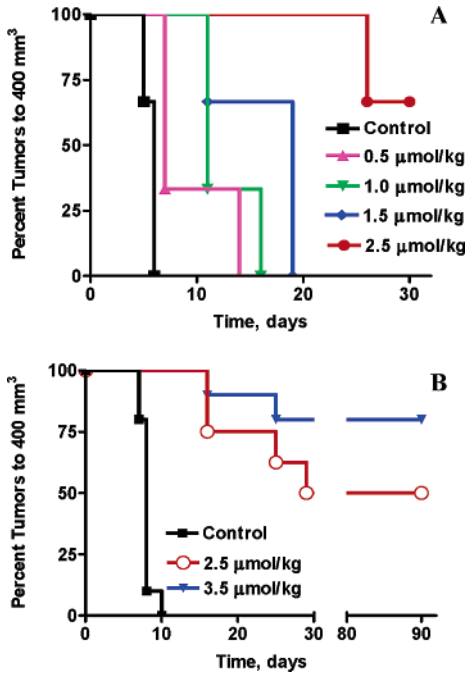

Figure 4. In vivo photosensitizing efficacy of conjugate **5** in C3H mice (10 mice/group) bearing RIF tumors and variable concentrations. The tumors were exposed to a laser light (665 nm, 135 J/cm^2) at 24 h after injection. (A) Drug concentrations = 0.5−2.5 μmol/kg. (B): Drug concentrations = 2.5 and 3.5 μmol/kg.

The organ distribution shown in Figure 6 confirms the whole mouse images. To quantitate the relative fluorescence intensity in each organ, we determined the mean fluorescent counts per organ, represented in a histogram format in Figure 6 (24, 48, and 72 h after injection). At 24 h, the probe is distributed in several organs, which confounds localization of the tumor by fluorescence imaging. However, 48 and 72 h after injection, the probe content in tumor is very high relative to the blood and to the different organs. The data demonstrate the high selectivity of the conjugate and clearly indicate the feasibility of identifying a tumor by optical imaging using a bifunctional cyanine photosensitizer probe.

Determination of Tumor/Skin Uptake Ratios and Skin Photosensitization. Persistence of photosensitizer

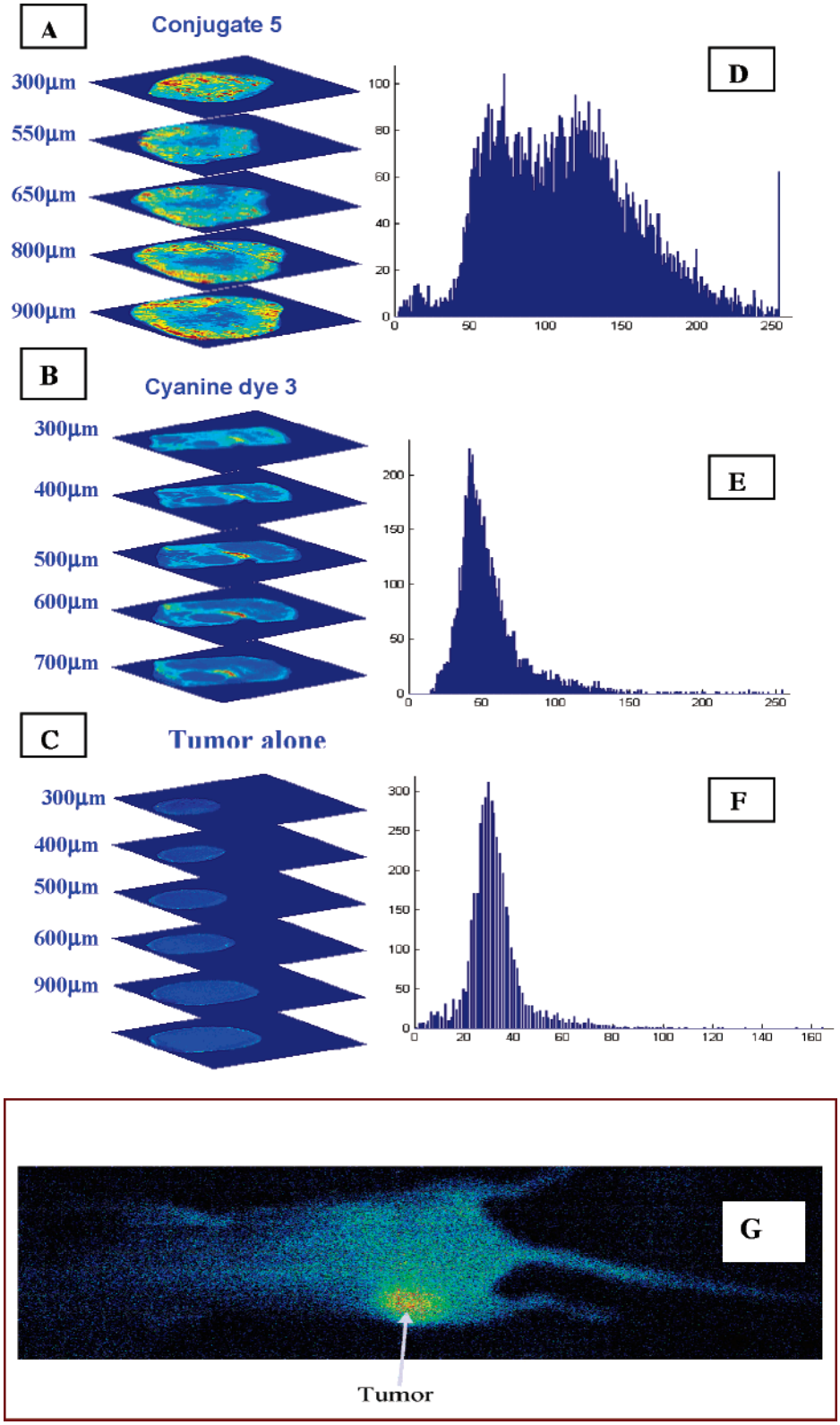

Figure 5. High-resolution tumor images at 24 h after injection: (A) conjugate **5** (3.5 μmole/kg), (B) cyanine dye **3** (3.5 μmole/kg), and (C) control (tumor alone). D, E, and F are their respective histograms (λ_{ex}, 780 nm; λ_{em}, 865 nm). (G) Localization of the conjugate **5** in a live mouse 24 h after injection (drug dose = 0.3 μmol/kg).

in the skin and resultant prolonged cutaneous photosensitivityhave been a major drawback for clinical PDT with porphyrin-based compounds (*49*). A high tumor:skin ratio of photosensitizer uptake therefore is critical for both tumor imaging and treatment.

The uptake of conjugate **5** (in tumor and skin) was determined by in vivo reflectance spectroscopy. In brief, conjugate **5** (3.5 μmol/kg) was injected into a C3H mouse bearing RIF tumors, and the in vivo absorption spectra of the conjugate present in tumor and skin were recorded at various time intervals by following the methodology routinely used in our laboratory. As can be seen from Figure 7A, the conjugate **5** produced a significantly higher uptake in tumor than skin at 24 h after injection.

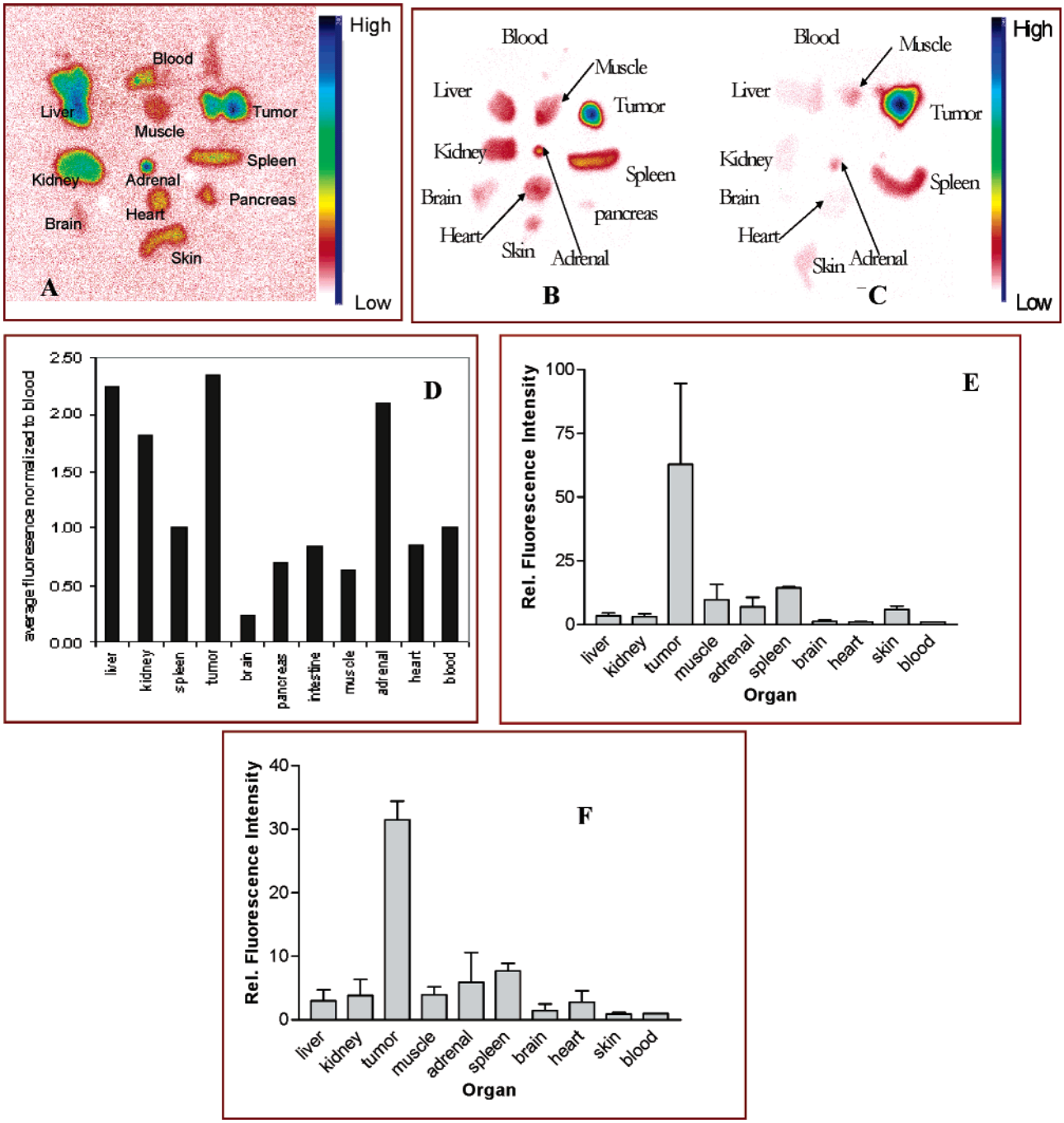

Figure 6. A, B, C: Images of the distribution of **5** in various organ parts at 24, 48, and 72 h after injection, respectively (drug dose = 3.5 μmol/kg). D, E, F: Relative fluorescence of conjugate **5** in selected organs at 24, 48, and 72 h after injection (2 mice/group). All intensities are relative to blood.

In a tumor, a substantial increase in drug uptake was observed from 24 to 48 h without a concomitant change in skin uptake. After 48 h, the drug concentration in tumor and skin began to decline, reaching negligible levels in the skin by 72 h while still maintaining relatively high tumor levels (Figure 7A). In contrast, as shown in Figure 7B, the cyanine dye **3** did not show any tumor selectivity and it cleared rapidly from tumor and skin, suggesting a remarkable difference in pharamacokinetic characteristics of the two compounds.

To validate the finding of low skin drug levels, general skin phototoxicity was assessed. The HPPH−cyanine dye conjugate **5** at a dose of 3.5 μmol/kg (therapeutic dose) was compared with HPPH and Photofrin at approximately equi-effective therapeutic doses. In each experiment, the mice (3 mice/group) were restrained without anesthesia in holders designed to allow the exposure of one hind foot. The foot was exposed to solar-simulated light for 30 min, either 24, 48, 72, and 96 h after injection. Foot response was judged using a 0−3 scale. As can be seen from Figure 7C, conjugate **5** had a minimal, transient response (score 0.1 24 h after injection) with no photosensitizing activity 48 h after injection, whereas HPPH at a 7.4-fold lower dose had greater skin phototoxicity 72 h after administration (Figure 7D). In contrast, Photofrin caused very significant phototoxicity, with scores of 1.5 (24 h), 1.5 (48 h), 1.4 (72 h), and 1.25 (96 h) (data not shown). These functional data confirm the imaging and absorption findings.

Effects on the Vasculature. In PDT-mediated therapy, it has been shown that vascular destruction in the tumor and immediate tumor-surrounding tissue can

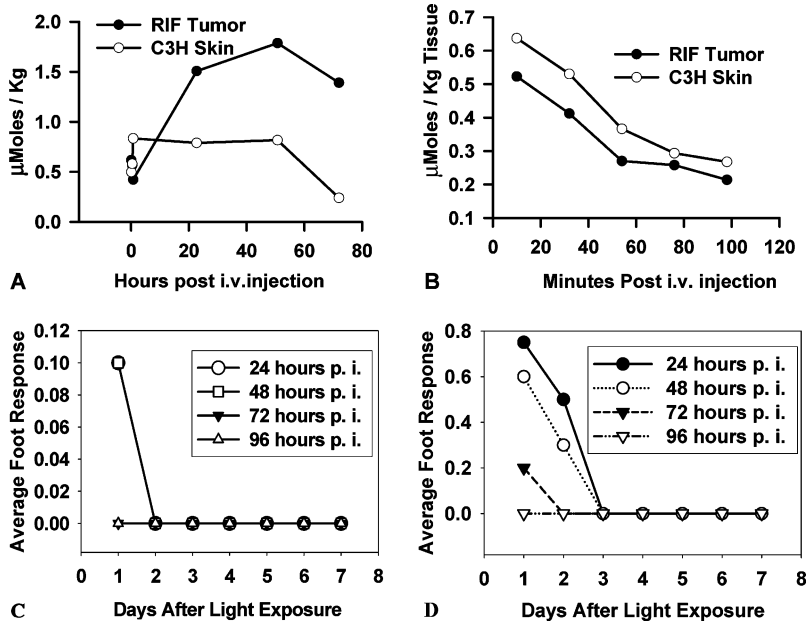

Figure 7. A and B: Tumor vs skin uptake of conjugate **5** and cyanine dye **3**, respectively, in C3H mice bearing RIF tumors at variable time points. C and D: Foot response in Swiss mice as a function of time after light and time interval between injection and light: (C) effect of conjugate **5** vs (D) HPPH on foot response at respective therapeutic doses (**5**, 3.5μmole/kg; HPPH, 0.47 μmol/kg) at various time intervals (for details see the text).

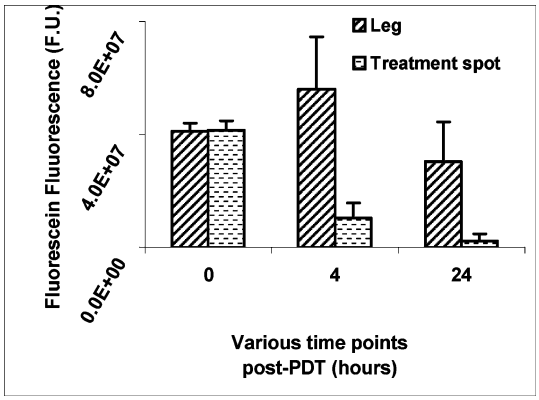

Figure 8. Vascular shutdown results obtained by fluorescein exclusion assay at 4 and 24 h after PDT.

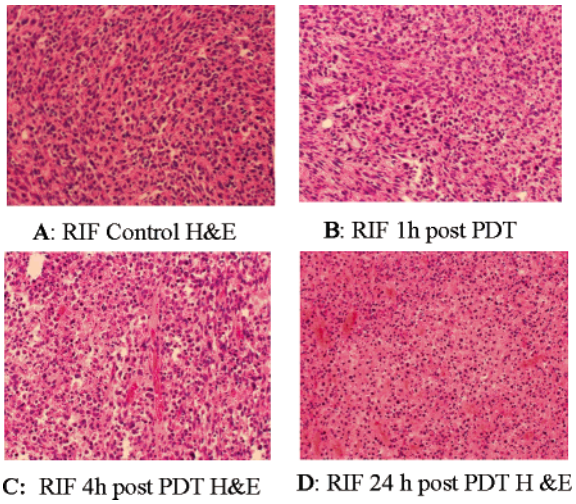

Figure 9. Histological analyses of conjugate **5** (after PDT). The dilated vessels at 4 h and necrosis at 24 h are evident.

contribute significantly to tumor control (*50*, *51*). Therefore, we determined the effects of the conjugate on the cutaneous vasculature. Conjugate **5** was injected intravenously, and 24 h later the mice in groups of three were treated with laser light at 665 nm for a total light dose of 135 J/cm^2 at a fluence rate of 75 mW/cm^2 (1 cm^2 diameter spot). The mice were evaluated for PDT-induced changes in vascular perfusion at various time points after PDT (0, 4, and 24 h) by injecting 0.20 cm^3 fluorescein (ex, 490 nm; em, 520 nm) intravenously as a perfusion marker. An in vivo fluorescence probe was then utilized to quantitate fluorescein fluorescence in the treatment site as compared to a nonlight treatment site. Each column represents the mean from three mice at each time point in comparison to the nontreated site.

As can be seen by Figure 8, immediately after PDT there is no difference in fluorescein fluorescence when comparing the drug/light treatment site to an unirradiated site of the leg.

However, at 4 and 24 h after PDT, there is a significant difference, with minimal to nearly no fluorescein fluorescence in the treated site, indicating that fluorescein was unable to penetrate due to vascular destruction. Histologic analysis confirmed this conclusion showing dilated and obstructed vessels, progressing toward hemorrhagic necrosis (Figure 9).

CONCLUSION

Our results indicate that (a) tumor-avid porphyrin-based compounds can be used as vehicles to deliver the optical imaging agent to tumor, (b) the inherent characteristics of two chromophores complement each other and their individual characteristics can be used for tumor detection and therapy, and (c) the presence of the cyanine dye appears to further improve the pharmacokinetics of the molecule, resulting in even faster clearance from the skin and elimination of prolonged skin phototoxicity, a major drawback associated with most porphyrin-based photosensitizers.

Our approach provides a unique opportunity for developing more tumor-specific, bifunctional agents for tumor detection and therapy by targeting those receptors known for high expression in tumors. Currently, the syntheses and biological studies of such target-specific

bifunctional agents containing more tumor-avid photosensitizers than HPPH and exhibit long-wavelength absorptions in the range of 700−800 nm are in progress.

ACKNOWLEDGMENT

The financial support from the NIH (CA55792), Roswell Park Alliance Foundation, and shared resources of the RPCI Support Grant (P30CA16056) is appreciated. One of the authors (A.G.) thanks the National Science Foundation under the Integrative Graduate Education and Research Traineeship (Grant DGE0114330) for the graduate fellowship.

LITERATURE CITED

(1) Henderson, B. W., and Dougherty, T. J. (1992) How does photodynamic therapy work. *Photochem. Photobiol. 55* (1), 145−157.

(2) Dougherty, T. J., Gomer, C., Henderson, B. W., Jori, G., Kessel, D., Korbelik, M., Moan, J., and Peng, Q. (1998) Photodynamic Therapy. *J. Natl. Cancer Inst*. *90*, 889.

(3) Dolmans, D. E. J. G. J., Fukumura, D., and Jain, R. K. (2003) Photodynamic Therapy for Cancer. *Nat. Rev., Cancer 3* (5), 380.

(4) Dougherty, T. J., and Levy, J. G. (2002) Photodynamic Therapy (PDT) and clinical applications. *Biomedical Photonics Handbook* (Vo-Dinh, T., Ed.), CRC Press, Boca Raton.

(5) Chen, Y., Li, G., and Pandey, R. K. (2004) Synthesis of bacteriochlorins and their potential utility in photodynamic therapy (PDT). *Curr. Org. Chem. 8* (12), 1105−1134.

(6) Ali, H., and van Lier, J. E. (1999) Metal complexes as photo- and radiosensitizers. *Chem. Rev*. *99*, 2379−2450.

(7) Pandey, R. K. (2002) Synthetic strategies in designing porphyrin-based photoensitizers for photodynamic therapy. In *Biomedical Photonics Handbook* (Vo-Dinh, T., Ed.), CRC Press, Boca Raton.

(8) Schmidt-Erfurth, U., Diddens, H., Birngruber, R., and Hasan, T. (1997) Photodynamic targeting of human retinoblastoma cells using covalent low-density lipoprotein conjugates. *Br. J. Cancer 75*, 54−61.

(9) Finger, V. H., Guo, H. H., Lu, Z. H., and Peiper, S. C. (1997) Expression of chemokine receptor by endothelial cells: detection bu intravital microscopy using chemokine-located fluorescent microspheres. *Methods Enzymol. 18*, 148−158.

(10) Hombrecher, H. K., Schell, C., and Thiem, J. (1999) Synthesis and investigation of galactopyranosyl-cholesterloxy substituted porphyrins. *Bioorg. Med. Chem. Lett. 6*, 1199−1202.

(11) Donald, P. J., Cardiff, R. D., He, D., and Kendell, K. (1991) Monoclonal antibody-porphyrin conjugate for head and neck cancer, the possible magic bullet. *Otolaryng. Head Neck 105* (6), 781−787.

(12) Hamming, A. W., Davis, N. L., Dubois, B. Quenville N. F., and Finley R. J. (1993) Photodynamic therapy of squamous cell carcinoma. An evaluation of a new photosensitization agent, benzoporphyrin derivatives and a new photoimmunoconjugate. *Surg. Oncol., 2* (3), 187−196.

(13) Vrouenraets, M. B., Visser, G. W. M., Stewart, F. A., Stigter, M., Oppelaar, H., Postmus, P. E., Snow, G. B., and van Dongen, G. A. M. S. (1999) Development of meso-tetrahydroxyphenyl-chlorin-monoclonal antibody conjugate for photoimmunotherapy. *Cancer Res*. *59*, 1505−1513.

(14) Karagianis, G., Reiss, J. A. Marchesini, R., DeCesare, M., Zunino, F., and Philips, D. R. (1996) Biophysical and biological evaluation of porphyrin-bisacridine conjugates. *Anti Cancer Drug Des. 11*, 205−220.

(15) Bachor, B. S., Shea, C. R., Gillis, R., and Hasan, T. (1991) Photosensitized destruction of human bladder carcinoma cells treated with chlorine6-conjugated microspheres. *Proc. Natl. Acad. Sci. U.S.A. 88*, 1580−1584.

(16) Li, G., Pandey, S. K., Graham, A., Dobhal, M. P., Mehta, R., Chen, Y., Gryshuk, A., Olson, K., Oseroff, A., and Pandey, R. K. (2004) Functionalization of OEP-based benzochlorins to develop carbohydrate-conjugated photosensitizers. Attempt to target β-galactoside-recognized proteins. *J. Org. Chem. 69*, 158−172.

(17) Pandey, R. K, Sumlin, A. B, Potter, W. R, Bellnier, D. A, Henderson, B. W, Constantine, S., Aoudia, M., Rodgers, M. A. J, Smith, K. M., and Dougherty, T. J. (1996) Structure and photodynamic efficacy among alkyl ether analogues of chlorophyll-a derivatives. *Photochem. Photobiol. 63*, 194−205.

(18) Henderson, B. W., Bellnier, D. A., Graco, W. R., Sharma, A., Pandey, R. K., Vaughan, L., Weishaupt, K. R., and Dougherty, T. J. (1997) A quantitative structure−activity relationship for a congeneric series of pyropheophorbide derivatives as photosensitizers for photodynamic therapy. *Cancer Res*. *57*, 4000−4007.

(19) Zheng, G., Potter, W. R., Sumlin, A., Dougherty, T. J., and Pandey, R. K. (2000) Photosensitizers related to purpurin-18-N-alkylimides: A comparative in vivo tumoricidal ability of ester versus amide functionalities. *Bioorg. Med. Chem. Lett. 10*, 123−127.

(20) Rungta, A., Zheng, G., Missert, J. R., Potter, W. R., Dougherty, T. J., and Pandey, R. K. (2000). Purpurinimides as photosensitizers: Effect of the presence and position of the substituents in in vivo photodynamic efficacy. *Bioorg. Med. Chem. Lett. 10*, 1463−1466.

(21) Zheng, G., Potter, W. R., Camacho, S. H., Missert, J. R., Wang, G., Bellnier, D. A., Henderson, B. W., Rodgers, M. A. J., Dougherty, T. J., and Pandey, R. K. (2001) Synthesis, photophysical properties, tumor uptake and preliminary in vivo photosensitizing efficacy of a homologous series of 3-(1′-alkyloxy)ethyl-3-devinylpurpurin-18-N-alkylimides with variable lipophilicity. *J. Med. Chem*. *44*, 1540−1559.

(22) Gryshuk, A. L., Graham, A., Pandey, S. K., Potter, W. R., Missert, J. R., Oseroff, A., Dougherty, T. J., and Pandey, R. K. (2002) A first comparative study of purpurinimide-based fluorinated vs nonfluorinated photosensitizers for photodynamic therapy. *Photochem. Photobiol. 76* (5), 555−559.

(23) Chen, Y., Graham, A., Potter, W., Morgan, J., Vaughan, L., Bellnier, D. A., Henderson, B. W., Oseroff, A., Dougherty, T. J., and Pandey, R. K. (2002) Highly stable and potent photosensitizers for photodynamic therapy. *J. Med. Chem. 45* (2), 255−258.

(24) Li, G., Graham, A., Chen, Y., Dobhal, M. P., Morgan, J., Zheng, G., Kozyrev, A., Oseroff, A., Dougherty, T. J., and Pandey, R. K. (2003) Synthesis, comparative photosensitizing efficacy, human serum albumin (site II) binding ability and intracellular localization characteristics of novel benzobacteriochlorins derived from vic-dihydroxybacteriochlorins. *J. Med. Chem. 46*, 5349−5359.

(25) Chen, Y., Sumlin, A., Morgan, J., Gryshuk, A., oseroff, A., Henderson, B. W., Dougherty, T. J., and Pandey, R. K. (2004) Synthesis and photosensitizing efficacy of isomerically pure bacteriopurpurinimides. *J. Med. Chem. 47*, 4814−4817.

(26) Dougherty, T. J., Pandey, R. K., Nava, H. R., Smith, J. A., Douglass, H. O., Edge, S. B., Bellnier, D. A., O'Malley, L., Cooper, M. (2000) Preliminary clinical data on a new photodynamic therapy photosensitizers HPPH for treatment of obstructive esophageal cancer. *Proc. SPIE 3009*, 25−27.

(27) Bellnier, D. A., Greco, W. R., Loewen, G. M., Nava, V., Oseroff, A. Pandey, R. K., Tsuchida, T., and Dougherty, T. J. (2003) Population pharmacokinetics of the photodynamic therapy agent HPPH in cancer patients. *Cancer Res. 63*, 1806−1813.

(28) Zhang, Z., Blesington, D., Hui, L., Busch, T. M., Glickson, J., Juo, Q., Chance, B., and Zheng, G. (2004) Redox ratio of mitochondria as an indicator for the response of photodynamic therapy. *J. Biomed. Opt. 9* (4), 772−778 and references therein.

(29) Harisingham, M. G., Willenberg, J., and Weissleder, R. (2003) *Primer of Diagnostic Imaging*, 3rd ed.; Elsevier.

(30) Sevick-Muraca, E. M., Kuwana, E., Godavarty, A., Houston, J. P., Thompson, A. B., and Roy, R. (2002) Near-infrared fluorescence imaging and spectroscopy in random media and tissues. Chapter 33 in *Biomedical Photonics Handbook* (Vo-Dinh, T., Ed.), CRC Press, Boca Raton.

(31) Lobel, J., MacDonald, I. Ciesielski, M. J., Barone, T., Potter, W. R., Pollina, J., Plunkett, R. J., Fenstermaker, R. A., and

Dougherty, T. J. (2001) 2-(1-hydroxyethyl)-2-devinylpyropheophorbide-a (HPPH) in a nude rat glioma model: implications for photodynamic therapy. *Laser Surg. Med*. *29* (5), 397−405.

(32) Garfinkel, M., Thomson, A. B., Ralston, W., Troy, T. L., Moore, T. A., Gust, J. D., Tatman, D., Reynolds, J. S., Muggenburg, B., Nikula, K., Mayer, R. H., Hawrysz, D. J., and Sevick-Muraca, E. (2000) Pharmacokinetics of indocyanine green and carotene-HPPH conjugate for detection of normal and tumor tissue using fluorescence, near-infrared continuous wave imaging. *Photochem. Photobiol. 72*, 94−102 and references therein.

(33) Majumdar, S. R., Majumdar, R. B., Grant, C. M., and Waggoner, A. S. (1996) Cyanine-labeling reagents: sulfobenzindocyanine succinimidyl esters *Bioconjugate Chem*. *7*, 356−362.

(34) Strekowski, L., Mason, C. J., Lee, H., Gupta, R., Sowell, J., and Patonay, G. (2003) Synthesis of water-soluble near-infrared cyanine dyes functionalized with 9succiniimdioxyl)-carbonyl group. *J. Heterocycl. Chem. 40*, 913−916.

(35) Tung, C. H., Lin, Y., Moon, W. K., and Weissleder R. A. (2002) A receptor-targeted near-infrared fluorescence probe in in vivo tumor imaging. *Chembiochem. 8*, 784−786.

(36) Becker, A., Hessenius, C., Licha, K, Ebert, B., Sukowski, U., Semmler, W., Wiedenmann, B., and Grotzinger, C. (2001) Receptor-targeted optical imaging of tumors with near-infrared fluorescent ligands. *Nature Biotechnol. 19*, 327−331.

(37) Ohulchanskyy T. Y., Donnelly D. J., Detty M. R., and Prasad P. N. (2004*)* Heteroatom substitution induced changes in excited-state photophysics and singlet oxygen generation in chalcogenoxanthylium dyes: effect of sulfur and selenium substitutions. *J. Phys. Chem. B 108*, 8668−8672.

(38) Kessel, D., Luo, Y., Deng, Y., and Chang, C. K. (1997) The role of subcellular localization in inhibition of apoptosis by photodynamic therapy. *Photochem. Photobiol. 65* (3), 422−426.

(39) Kawada, K., Yonei, T., Ueoka, H., Kiura, K., Tabata, M., Takigawa, N., Harada, M., and Tanimoto, M. (2002) Comparison of chemosensitivity tests. Clonogenic assay versus MTT assay. *Acta Med. Okayama 56* (3), 129−134.

(40) Patterson, M. S., Hayward, J. E., Farrell, T. J., and Wilson, B. C. A general purpose instrument for PDT dosimetry. *SPIE* 2371, 477−481.

(41) Bellnier, D. A. (1991) Potentiation of photodynamic therapy in mice with recombinant human tumor necrosis factor-a. *J. Photochem. Photobiol. 8*, 203−210.

(42) Bellnier, D. A., Potter, W. A., Vaughan L. A., Sitnik T. M., Parsons, J. C., Greco, W. R., Whitaker J., Johnson, P., and Henderson, B. W. (1995) The validation of a new vascular damage assay for photodynamic therapy agents. *Photochem. Photobiol. 62* (5), 596−905.

(43) Henderson, B. W., Vaughan, L., Bellnier, D. A., and Oseroff, A. R. (1995) photosensitization of murine tumor, vasulature and skin by 5-aminolevulinic acid induced porphyrin. *Photochem. Photobiol*. *62*, 780−789.

(44) Kessel, D., and Luo, Y. (1998) Mitochondrial photodamage and PDT-induced apoptosis. *J. Photochem. Photobiol. B 42* (2), 89−95.

(45) Morgan, J., and Oseroff A. R. (2001) Mitochondria-based anti-cancer photodynamic therapy. *Advanced Drug Delivery Reviews-Drug and DNA delivery to mitochondria* (Eds. Weissig and Torchilin, V. P.), *49*, 71−86.

(46) MacDonald, I., and Dougherty, T. J. (2001) Basic principles of photodynamic therapy. *J. Porphyrin Phthalocyanines 5* (2), 105−129.

(47) Chance, B., Schoener, B., Oshino, R., Itshak, F., and Nakase, Y. (1979) Oxidation−reduction ratio studies of mitochondria in freeze-trapped samples and flavoprotein fluorescence signals. *J. Biol. Chem. 254* (11), 4764−4771.

(48) Achilefu, S., Jimenez, H. N., Dorshow, R. B., Bugaj, J. E., and Webb, E. G. (2002) Synthesis, in vitro receptor binding and in vivo evaluation of fluorescein and carbocyanine peptide-based optical contrast agents. *J. Med. Chem. 45*, 2003−2015.

(49) Belliner, D. A., Greco, W. R., Parsons, J. C., Oseroff, A., Kuebler, A., and Dougherty, T. J. (1997) An assay for the quantitation of Photofrin in tissues and fluids. *Photochem. Photobiol. 66*, 237−244.

(50) Fingar, V. H., Siegel, K. A., Wieman, T. J., and Doak, K. W. (1993) The effect of thromboxane inhibitors on the microvascular and tumor response to photodynamic therapy. *Photochem. Photobiol. 58*, 393−399.

(51) Dolman, D. E. J. G., Kadambi, A., Hill, J. S., Flores, K. R., Gerber, J. N., Walker, J. P., Borel Rinkes, I. H. M., Jain, R. K., and Fukumura, D. (2002) Targeting Tumor Vasculature and Cancer Cells in Orthotopic Breast Tumor by Fractionated Photosensitizer Dosing Photodynamic Therapy. *Cancer Res. 62*, 4289−4294.

BC050177O